Journal of the European Ceramic Society **15** (1995) 127–133

0955-2219/95/$9.50

Laser Ablation of Barium Titanate Ceramics Prepared by the Citric Route: The Evolution of Residual Carbon Content

C. Miot,[a] C. Proust,[a,b] E. Husson,[a,b] G. Blondiaux[c] & J. P. Coutures[a]

[a] CRPHT-CNRS, 45071 Orléans cedex 2, France
[b] LPMM, ESEM, Université d'Orléans, B.P. 6747, 45067 Orléans cedex 2, France
[c] CERI-CNRS, 45071 Orléans cedex 2, France

(Received 15 February 1994; revised version received 24 June 1994; accepted 8 July 1994)

Abstract

The laser-induced ablation mechanism of $BaTiO_3$ ceramics has been followed by SEM and EPMA analyses. The evolution of the residual carbon content has been studied by $^{12}C(d,p)^{13}C$ nuclear technique under a 10^{-9} mbar vacuum with laser powers below and above the ablation threshold. The residual carbon remains constant for laser powers below the ablation threshold and is ejected from the crater formed and partly deposited around it when ablation occurs. Immediately after the end of laser ablation, the residual carbon diffuses from the bulk to the surface of the ceramic, leading to high C concentrations in the whole ceramic surface layer. The chemical form of carbon and its mobility in such ceramics are discussed.

1 Introduction

Residual carbon remaining in ceramic materials after the sintering step, originating from the use of organic precursors during the powder fabrication, may influence the material properties. In a previous paper,[1] the residual carbon content has been evaluated in $BaTiO_3$ ceramics. It was shown that the C content is about 50 ppm by weight in the ceramic bulk and that it increases at the surface which exhibits a concentration of several hundreds or thousands of ppm. The surface layer carbon could have two origins: an atmospheric contamination carbon adsorbed at the surface of the ceramic, and material intrinsic carbon, the concentration of which depends on the shape of ceramic pieces and the sintering temperature.

Laser ablation is becoming increasingly significant in materials processing techniques with which to obtain thin films. However, in spite of the scientific and technological importance of this process, relatively little has been published about the physical and chemical mechanisms of laser-induced desorption and ablation from these materials.[2–4] Recent works on laser ablation of $BaTiO_3$[5–11] or other perovskite oxides,[12–15] performed under partial pressure of O_2, are only interested in the production of thin films with a good stoichiometry or a preferred orientation[16] and a little has been published about bulk ceramics.

It seems appropriate to (i) study the ablation mechanism by the evolution of the microstructure by scanning electron microscopy and local analyses by electron probe microanalysis as a function of the number or the power of laser shots, (ii) follow the evolution of the residual carbon content by the $^{12}C(d,p)^{13}C$ nuclear technique after laser-induced desorption and ablation, as a function of the time under an ultra-high vacuum or in air, (iii) discuss the mobility and the chemical form of the residual carbon.

2 Experimental

2.1 Samples

$BaTiO_3$ powders were obtained by a citric resin method, described in previous papers.[17–19] The mixed citrate $BaTi(C_6H_6O_7)_3\ 6H_2O$ is prepared and then dissolved in a mixture of citric acid, ethylene glycol and water with the ratio of $BaTiO_3$ mass/solution mass (R) being 1%. This mixture was calcined at 700°C in static air and gave pure $BaTiO_3$ powders after 2 h. After an ultrasonic deagglomeration step, powders were pressed to give discoidal samples, then they were sintered in

air at 1300°C or 1400°C for 2 h with a heating rate of 300°C/h up to 600°C then 70°C/h up to 1300°C or 1400°C. Sintered discs were about 1·8 cm diameter and 1 mm thick.

2.2 Laser device

The laser ablation was performed at room temperature in an ultra-high vacuum (UHV) chamber with a pressure of about 10^{-9} mbar. Samples were mounted on a micromanipulator and placed in the UHV chamber. A YAG laser with a pulse width of 7 ns and a doubled output (532 nm) was used. Average energy levels were between 20 and 70 mJ producing powers of between 1·4 and 8·6 $\times$ 10^7 W/cm^2 on the sample. The diameter of the laser spot was between about 2 and 5 mm.

2.3 EPMA analysis

Electron probe microanalysis (EPMA) semi-quantitative measurements were performed with a Cameca instrument with a voltage of 10 kV and an intensity of 30 nA under a vacuum of 10^{-5} mbar. The detectors used were PET for Ti ($K_{\alpha 1}$ radiation) LiF for Ba ($L_{\alpha 1}$ radiation) and PC2 for C (K_α radiation). The ablated ceramics were metallized with nickel. The depth analyzed was about 0·2 μm and the surface was a few μm in diameter, thus it was possible to focus the electron incident beam on a ceramic grain. The results given have been averaged over several tens of measurements.

2.4 Raman spectroscopy

Raman spectra of the ablated ceramics were performed with a Dilor Raman microprobe using the 514·5 nm wavelength of a Ar^+ laser with a power of several hundreds of mW. The area and depth analyzed were about 1 μm.

2.5 Carbon analysis

The carbon concentration analysis was carried out by $^{12}C(d,p)^{13}C$ nuclear technique using deuterons from the Van-de-Graaff accelerator of the Centre d'Etude sur les Radiations Ionisantes (CERI). The method has been described in different articles.[20–22] The measurements were performed at 950 keV and 1420 keV deuteron energy in a UHV chamber with a vacuum of about 10^{-9} mbar. The detector was a diode with an active surface of 300 mm^2 situated 64 mm from the sample position and protected by a 20 μm thick Al foil. The detection angle θ was 150°. The beam current was 10 nA. A collimator was placed at the entry of the UHV chamber and 60 mm from the target, giving a constant deuteron beam diameter of 7 mm^2. The counting time was about 20 min per data point.

For 950 keV energy incident deuterons, the carbon content (t) is given in g/cm^2 by the formula:

$$t = \frac{dA}{\Phi} * \frac{1}{\frac{d\sigma}{d\Omega}} * \frac{1}{d\Omega} * \frac{M}{N}$$

where dA = number of detected particles = reaction peak area; Φ = number of incident particles = $Q/1{\cdot}6 \times 10^{-19}$ with Q = total incident charge measured by the integrator (C); $d\sigma/d\Omega$ = differential cross-section (cm^2/sr/nucleus); $d\Omega$ = solid angle determined by the detector and the impact point of the beam on the target (sr); M = atomic mass of the studied nucleus (g/mol); and N = Avogadro number. The differential cross-section has been taken equal to 30 mbarns according to Ref. 23. The solid angle is $7{\cdot}32 \times 10^{-2}$ sr.

Taking into account the density of the ceramics and the depth of the material analyzed (0·4 μm), it is possible to deduce the carbon content in ppm (by weight) in the surface layer.

For 1420 keV energy incident deuterons, a surface carbon content (0·4 μm depth) has been evaluated taking a cross-section of 40 mbarns, then, if it is assumed that there is no gradient of concentration as a function of the depth, the carbon content of the subsurface (between 0·4 and 4·4 μm) may be evaluated taking an average cross-section of 64 mbarns.

3 Results

The sintered ceramics had densities approaching 99% of the theoretical density (d_{th} = 6·02 g/cm^3) and SEM observations showed an average grain size of about 100 μm.

3.1 Ablation mechanism

The physical phenomena that occur when a laser beam is focused onto a material surface depend mainly on (i) the power of the laser beam, (ii) the thermal properties of the material and (iii) the absorptivity of the material at the wavelength used. According to Sankur & Cheung,[24] three power density regimes can be defined: low (<10^6 W/cm^2), intermediate (>10^6 and <10^6 W/cm^2) and high (>10^8 W/cm^2). In the low power density regime, surface melting and evaporation are under quasi-equilibrium conditions. In the high power density regime a plasma is formed. In the intermediary regime, the plasma contribution is small but dissociated species are observed in the evaporation stream. The present experimental conditions, with a laser power of about 10^7 W/cm^2, correspond to this last case

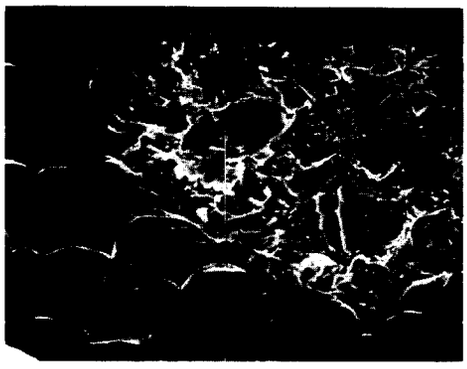

Fig. 1. SEM image of a $BaTiO_3$ ceramic damaged by 100 shots at $2{\cdot}7 \times 10^7$ W/cm^2. Grain explosion is observed without the appearance of a molten zone.

Fig. 3. SEM image of a $BaTiO_3$ ceramic damaged by 100 shots at $3{\cdot}9 \times 10^7$ W/cm^2. The first molten zones appear at triple grain boundaries and at pores, in addition to grain explosion.

The ablation phenomenon was followed by SEM by using increasing powers of the laser beam and numbers of shots.

Firstly, a series of 100 laser shots with variable powers was performed onto as-sintered ceramic surfaces. In order to avoid interactions of one series of shots with another one, a new ceramic sample was used for each series.

For a laser power of $2{\cdot}7 \times 10^7$ W/cm^2, an explosion of the grains was observed without appearance of a molten zone (Fig. 1). Thus the ablation threshold is situated at about $2{\cdot}6 \times 10^7$ W/cm^2 in these conditions. At $3{\cdot}2 \times 10^7$ W/cm^2, the same phenomenon was observed (Fig. 2) but the ceramic was ablated to 4–5 μm depth. At $3{\cdot}9 \times 10^7$ W/cm^2, the first molten zones appeared at triple grain boundaries and at pores (Fig. 3) in addition to grain explosion and an ablation depth of about 5 μm. For higher laser powers (experiments were performed at 5·1 and $7{\cdot}7 \times 10^7$ W/cm^2) only molten zones were observed with very irregular features (Fig. 4). As the laser power increases, the formation of a more and more regular crater is observed: a regular form 200–300 μm deep is obtained for laser powers of $5{\cdot}7$–$7{\cdot}1 \times 10^7$ W/cm^2. The ablation depth was roughly evaluated during SEM observations.

The influence of the number of shots at constant laser power was studied. Two values for the laser power were chosen: $2{\cdot}7$ and $5{\cdot}7 \times 10^7$ W/cm^2. A series of 500 shots at $2{\cdot}7 \times 10^7$ W/cm^2 showed, in addition to the grain explosion already mentioned for 100 shots at this laser power, a rise of grains from the surface due to the release of occluded gas (Fig. 5). Even for a number of shots greater than 500, no molten zone was observed. It seems that, below a certain laser power threshold, molten zones are never observed. Finally, for 500 shots at $5{\cdot}7 \times 10^7$ W/cm^2, the formation of a regular crater is clearly observed: Fig. 6 shows the different zones at the surface of the ceramic:

(i) The zone undamaged by the laser beam.
(ii) The circular zone around the crater, which is smooth and covered in places by more or less spherical nodules which seem to come from the crater center. Black soot-like deposits are also observed. Sometimes holes like chimneys appear that are probably due to the release of gas.
(iii) The crater bottom with a very damaged surface: the erosion seems to always originate at the pores and at the triple grain boundaries.

If the laser beam power is increased (up to $9{\cdot}3 \times$

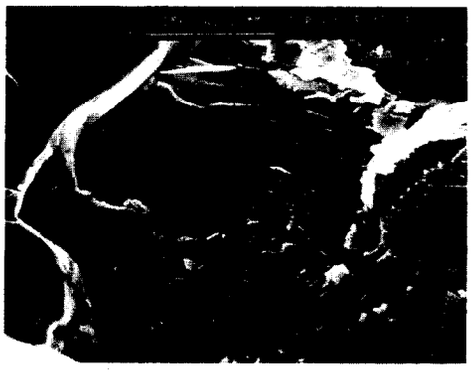

Fig. 2. SEM image of a $BaTiO_3$ ceramic damaged by 100 shots at $3{\cdot}2 \times 10^7$ W/cm^2. The ceramic is ablated to a depth of 4–5 μm.

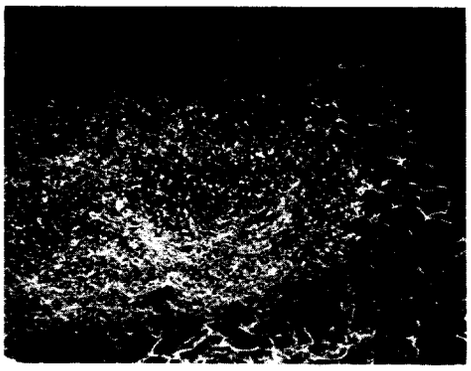

Fig. 4. SEM image of a $BaTiO_3$ ceramic damaged by 100 shots at $4{\cdot}3 \times 10^7$ W/cm^2. Very irregular molten zones are observed.

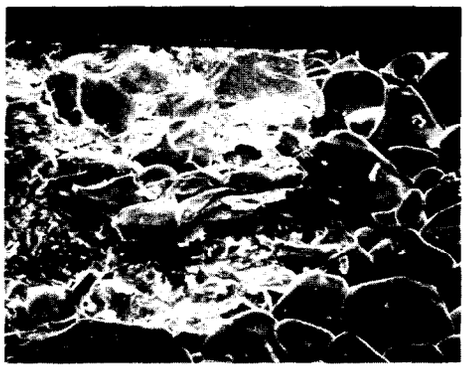

Fig. 5. SEM image of a $BaTiO_3$ ceramic damaged by 500 shots at $2{\cdot}7 \times 10^7$ W/cm^2. Grain explosion is observed as well as an upthrust of grains due to the release of occluded gas.

10^7 W/cm^2) or if the shot number is increased (up to 1500 shots) the observed phenomena are similar with the crater formed being much deeper.

3.2 Analysis of Ti and Ba compositions in ablated ceramics

Measurements of Ti and Ba contents have been performed by electron microprobe. Ceramics studied before laser treatment had a Ba/Ti ratio of $1{\cdot}03 \pm 0{\cdot}03$. The citric method used to produce the present ceramics gives, in principle, a Ba/Ti ratio equal to 1. The slightly higher value found may be explained because standards such as TiO_2 or $BaSO_4$ were not used to calibrate the measurements and because there probably exist interaction effects between Ti and Ba elements. This value is a relative value that is self-consistent and only its variation is studied.

A ceramic damaged by 500 laser shots at $5{\cdot}7 \times 10^7$ W/cm^2 was then analyzed. The crater bottom exhibits a Ba/Ti ratio of 1·25, the glossy, black circular zone around it has a ratio of 0·95 and the ejected particles a ratio of 1·08. The non-irradiated part of the ceramic exhibits a ratio of 1·03. Thus, the crater and the ejected particles are richer in Ba whereas the black circular zone is richer in Ti than the stoichiometric composition.

Measurements have also been performed by Rutherford back-scattering (RBS) technique on such a ceramic. A very slight decrease of the Ti content in the crater confirmed the electron microprobe measurements.

3.3 Analysis of the carbon content by $^{12}C(d,p)^{13}C$

Measurements performed on as-sintered ceramics at a 950 keV deuteron energy gave a carbon content of 90 ng/cm^2 in the surface layer (0·4 μm), corresponding to about 350 ppm.[1] Then, the authors tried to desorb the surface carbon by laser-beam cleaning but no change in the C content was observed until the laser power was high enough to ablate the ceramic surface.

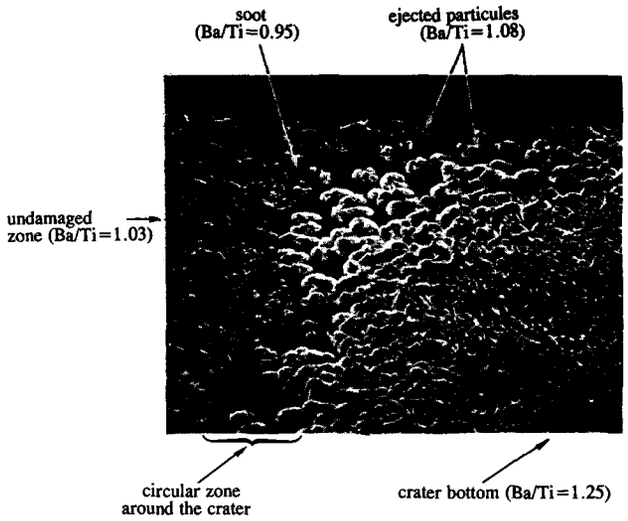

Fig. 6. SEM image of a $BaTiO_3$ ceramic damaged by 500 shots at $5{\cdot}7 \times 10^7$ W/cm^2. A regular crater is formed (200–300 μm depth) and different zones may be observed: the crater bottom, a circular zone around the crater with soot and ejected spherical particles and unperturbed surface.

Finally, ceramics damaged by 500 laser shots at $5{\cdot}7 \times 10^7$ W/cm^2 were studied. Taking into account the technical difficulties in focusing the laser and deuteron beams onto a given area, a large crater was formed by scanning the laser shots over a square of area 16 mm^2. The C content was measured in different areas of the damaged ceramics: in the crater center, around it and in unperturbed zones. The results are given in Table 1. It is observed that immediately after laser ablation, the C content is much smaller in the crater and higher in the glossy, black aureole around the crater, whereas the nonirradiated part of the ceramic exhibits a C content of about 350 ppm like the as-sintered ceramics. A measurement performed at 1420 keV energy in the crater showed also a very low carbon concentration. Thus the carbon does not migrate below the surface of the crater under the laser shots. There is, more probably, an ejection–redeposition mechanism.

The evolution of the carbon content of these ceramics left in a 10^{-9} mbar vacuum was observed, after 1·5 h, the C content had increased in all the

Table 1. Carbon content (in ppm) measured as a function of the time for areas for the ceramics with differing degrees of damage

Time	*Crater center*	*Around the crater*	*Undamaged surface*
Before laser shots[a]	350	350	350
After laser shots[a]	110	600	380
After 1·5 h[a]	180	840	560
After 72 h[a]	820	870	900
After 3 months[b]			
Surface	12000	6000	3000
Subsurface	830	100	100

[a] In UHV chamber.
[b] After an exposure to air for 3 months.

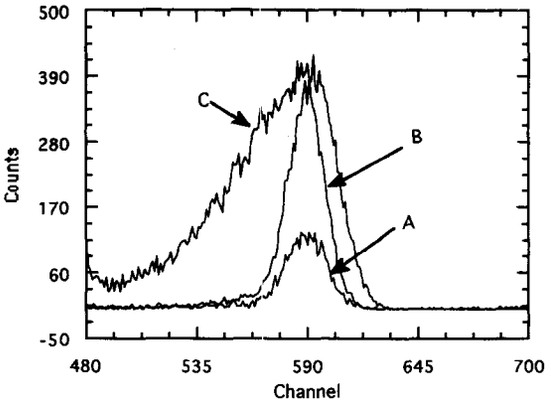

Fig. 7. The C peaks of the proton spectra of $^{12}C(d,p)^{13}C$ reaction obtained from 1420 keV incident deuteron energy: (A) far from the crater, (B) around the crater, (C) in the crater bottom. A symmetrical shape characterizes a C content much higher in the surface layer than in the bulk. The very unsymmetrical (C) peak reveals that C content is high both in the surface layer and in the bulk.

zones, particularly in the zone around the crater; after 72 h the C concentration was practically constant in the whole surface and increased by a factor close to 2·5 in comparison with the C content found in the as-sintered ceramics before laser shots. An equilibrium seemed to be established between the ceramic surface and the chamber atmosphere.

It was interesting to study the evolution of the C content with time after removing the ceramic from the UHV chamber of the apparatus. After an exposure in air for three months, $^{12}C(d,p)^{13}$ C measurements were performed in the same conditions in the UHV chamber with 950 keV energy incident deuterons. The results obtained are reported in Table 1. A strong increase of the surface carbon content was observed. The surface of the ceramic which was not damaged by the laser beam impact exhibits a C content of about 3000 ppm, whereas as-sintered ceramics of 1 mm thick generally exhibit a surface C content of about 350 ppm, a value remaining constant even after an exposure of several months in the air.[1] The surface around the crater and the crater bottom exhibit C contents of 6000 ppm and 12000 ppm respectively. These results were confirmed by EPMA analysis. In the crater bottom a large concentration of carbon was observed. $^{12}C(d,p)^{13}$ C measurements performed with 1420 keV energy incident deuterons showed that in the subsurface the C content is low (about 100 ppm) except in the crater center (830 ppm). The spectra given in Fig. 7 show the shape of the peaks: they are quasi-symmetrical for the measurements performed around the crater and further from it and very unsymmetrical for those performed in the crater center, this last profile is characteristic of a high C content both in the surface layer and in the bulk.

4 Discussion

Chan & Mazumder[2] have developed a model describing laser ablation damage. When an intense laser beam arrives at the target surface, different processes may occur. At the beginning of the laser pulse, the absorbed laser energy heats the target up to the melting point and then to the vaporization temperature. The vaporization generates a recoil pressure that pushes the vapour away from the target and expels the liquid sideways. Thus a part of the material is removed from the target both in vapor and liquid form. The absorbed laser energy should be partitioned into (i) loss into the target, (ii) latent heat of fusion and vaporization and (iii) creation of a recoil pressure to push the vapor away and expel the liquid.

In the present case, the circular zone exhibiting a glossy and black feature seems to be a consequence of the vapor ejection and lateral expulsion of the liquid. The ablation mechanism could be described as follows:

—Because of the high heating of the material, there is formation of a liquid and then vapor phases that are Ti-rich, the lightest elements being ejected first, as was observed by other workers.[14]

—The liquid phase deposited in the bottom of the crater or around it could correspond to the ultimate step before evaporation, the material not having reached a sufficient temperature to be volatilized.

—The ceramic grains which remain in the crater bottom or which have been ejected under the repeated laser shots on the surface around the crater are richer in heaviest elements, i.e. Ba in the present case.

Concerning the C content evolution after laser ablation, the same type of phenomenon is observed: the very light C element is eliminated when the ceramic is heated; thus the crater center exhibits a very low C content. One could think that C is totally evaporated when the vapor phase is formed; in fact, a relatively high C content is measured in the neighboring crater; the black color of the glossy zones could be due to the formation of carbon in a chemical form close to graphite, although this could not be confirmed by Raman microprobe. Thus carbon ejected from the crater is surely present in the vapor phase and also in the liquid phase.

The evolution of the C content with the time after laser ablation seems quite surprising. As ceramics are maintained in ultra-high vacuum conditions and the undamaged surface exhibits an increased C content, it seems more probable that

carbon comes from the bulk of the ceramic rather than from the chamber of the apparatus (although this last hypothesis could not be totally eliminated). Thus, it can be assumed that residual carbon is, in the sintered ceramic, in the form of chains; in the regions of the ceramics damaged by the laser thermal phenomenon, the C–C bonds should be broken and carbon become more mobile and diffuse to the surface of the ceramic.

After removing the ceramic from the UHV chamber and exposing it in the air for three months, the surface C content strongly increased, this phenomenon may have two origins:

(i) The observed carbon comes from the bulk of the ceramic; in this case the diffusion of carbon continues after 72 h in the UHV chamber.

(ii) The observed carbon results from the atmospheric contamination, the surface of the ceramic becoming more active under the laser bombardment. The measured C contents show in this case that this carbon is not totally desorbed when the ceramic is replaced in the UHV chamber to perform new measurements but seems quite well bonded to the ceramic.

At the present time, it is not possible to differentiate between these two points and further experiments are now in progress. In any case, the Raman microprobe spectra performed both on as-sintered and ablated ceramics showed that carbon is not present as carbonate, carbon dioxide or carbides but rather as hydrocarbon chains. XPS measurements could give more information about the chemical form of this carbon.

5 Conclusion

This work allowed the laser-induced ablation mechanism of $BaTiO_3$ ceramics to be followed and new information to be obtained about the residual carbon present in $BaTiO_3$ ceramics prepared by the citrate route. For laser powers below the ablation threshold, C is not desorbed by laser-beam cleaning, thus it seems well bounded or trapped in the material. For laser powers above the threshold ablation, C is ejected from the crater formed and deposited partly as soot around it. The laser beam–material interaction leads, after ablation, to an important diffusion of the carbon from the bulk of the ceramic to its surface. Residual carbon could be present in as-sintered ceramics in the form of hydrocarbon chains and the laser bombardment could break them and give much more mobile carbon or hydrocarbon species.

References

1. Proust, C., Husson, E., Blondiaux, G. & Coutures, J. P., Residual carbon detection in barium titanate ceramics by nuclear reaction technique. *J. Eur. Ceram. Soc.*, **14** (1994) 215–19.
2. Chan, C. L. & Mazumder, J., One-dimensional steady-state model for damage by vaporization and liquid expulsion due to laser–material interaction. *J. Appl. Phys.*, **62**, (1987) 4579–86.
3. Cheung, J. T. & Sankur, H., Growth of thin films by laser-induced evaporation. *Solid State Mater. Sci.*, **15**, (1988) 63–109.
4. Haglund, Jr, R. F., Tank, K. & Chen, C. H., Production of molecular clusters of lithium niobate by ultraviolet and visible laser abalation. *Mater. Res. Soc. Symp. Proc.*, **243** (1992) 405–10.
5. Nashimoto, K. & Fork, D. K., Epitaxial growth of MgO on GaAs(001) for growing epitaxial $BaTiO_3$ thin films by pulsed laser deposition. *Appl. Phys. Lett.*, **60**, (1992) 1199–201.
6. Davis, G. M. & Gower, M. C., Epitaxial growth of thin films of $BaTiO_3$ using excimer laser ablation. *Appl. Phys, Lett.*, **55** (1989) 112–14.
7. Roy, D. & Krupanidhi, S. B., Pulsed excimer laser ablated barium titanate thin films. *Appl. Phys. Lett.*, **61** (1992) 2057–9.
8. Gibson, U. J., Ruffner, J. A., McNally J. J. & Peterson, G., Nd: YAG laser ablation of $BaTiO_3$ thin films. *Mat. Res. Soc. Symp.*, **191** (1990) 19–24.
9. Norton, M. G. & Carter, C. B., Observation of the early stages of heteroepitactic growth of $BaTiO_3$ thin-films. *J. Mat. Res.*, **5** (1990) 2762–5.
10. Nashimoto, K., Fork, D. K., Ponce, F. A. & Tramontana, J. C., Epitaxial $BaTiO_3$/MgO structure grown on GaAs(100) by pulsed laser deposition. *Jpn. J. Appl. Phys.*, **32** (1993) 4090–102.
11. Cheng, H. F., Yeh, M. H., Liu, K. S. & Lin, I. N., Characteristics of $BaTiO_3$ films prepared by pulsed laser deposition. *Jpn. J. Appl. Phys.*, **32** (1993) 5656–60.
12. Tabata, H., Kawai, T., Kawai, S., Murata., O., Fujioka, J. & Minakata, S., Preparation of $PbTiO_3$ thin films at low temperature by an excimer laser ablation technique. *Appl. Phys. Lett.*, **59** (1991). 2354–6.
13. Hirano, T., Fujii, T., Fujino, K., Sakuta, K. & Kobayashi, T., Epitaxial $SrTiO_3$ thin films grown by ArF excimer laser deposition. *J. Appl. Phys.*, **31**, (1992) L511–14.
14. Haglund, Jr, R. F., Affatigato, M., Niehof, A. & Heiland, W., Ultraviolet laser ablation of halides and oxides. *Nucl. Inst. Methods Phys. Res. Sect. B*, (1992) 206–11.
15. Eyett, M., Bauerle, D., Wersing, W., Lubitz, K. & Thomann, H., Laser-induced chemical etching of ceramic $PbTi_{1-x}Zn_xO_3$ *Appl. Phys.*, **A40** (1986) 235–9.
16. Norton, M. G., Cracknell, K. P. B. & Carter, B., Pulsed-laser deposition of barium titanate thin films. *J. Am. Ceram. Soc.*, **75** (1992) 1999–2002.
17. Pechini, M., US Patent 3330 697, 1967.
18. Coutures, J. P., Odier, P. & Proust, C., Barium titanate formation by organic resins formed with mixed citrate. *J. Mater. Sci.*, **27**, (1992) 1849–56.
19. Proust, C., Husson, E., Odier, P. & Coutures, J. P., Sintering ability of $BaTiO_3$ powders elaborated by citric process. *J. Eur. Ceram. Soc.*, **12** (1993) 153–7.
20. Wengeler, H., Knobel, R., Kathrein, H., Freund, F., Demortier, G. & Wolff, G., Atomic carbon in magnesium oxide single crystals. Depth profiling, temperature- and time-dependent behavior. *J. Phys. Chem. Solids*, **43** (1982) 59–71.
21. Oberheuser, G., Kathrein, H., Demortier, G., Gouska, H. & Freund, F., Carbon in olivine single crystals analyzed by the $^{12}C(d,p)^{13}C$ method and by photoelectron

spectroscopy. *Geochim. Cosmochim. Acta*, **47** (1983) 1117–29.
22. Mathez, E.A., Carbon abundances in mantle minerals determined by nuclear reaction analysis. *Geophys. Res. Lett.* **11** (1984) 947–50.
23. Huez, M., Quaglia, L. & Weber, G., Fonction d'excitation de la réaction $^{12}C(d,p)^{13}C$ entre 400 et 1350 keV. Distributions angulaires. *Nucl. Instr. Methods*, **105** (1972) 197–203.
24. Sankur, H. & Cheung, J. T., Formation of dielectric and semiconductor thin films by laser-assisted evaporation. *Appl. Phys.*, (1988) **A47** 271–84.